Melting Order of Successively Longer Yeast Phenylalanine-Accepting Transfer Ribonucleic Acid Fragments with a Common 5′ End†

John A. Boyle,* Sung-Hou Kim, and Patricia E. Cole*,‡

ABSTRACT: Temperature-jump methods were used to study the kinetics of the helix to coil transition in three fragments of yeast $tRNA^{Phe}$ that share a common 5′ terminus (the 5′ end of the mature tRNA). Correlation of the extrapolated helix dissociation time constants with NMR exchange broadening results allows assignment of the structural basis of the optical melting transition in the fragments. The results confirm nuclear magnetic resonance findings on these fragments: the 5′ $^1/_4$ fragment has no helical structure; the 5′ $^1/_2$ fragment contains the D stem; and the 5′ $^3/_5$ fragment contains the D stem and the anticodon stem. These are the structures expected if sequential folding of the tRNA during biosynthesis were to occur. The D stem is the last helix to melt in the 5′ $^3/_5$ fragment. We suggest that structural elements in addition to the four Watson–Crick base pairs of the D-stem helix are responsible for the anomalously high T_m of that hairpin.

Specific small fragments of nucleic acids have proven useful in studies of the conformational properties of the larger macromolecules. In particular, defined fragments of tRNA have been used to evaluate the T_m of single hairpin helices and to support structural assignments of optical melting effects in the intact tRNA [see Wintermeyer et al. (1969), Römer et al. (1969), Riesner et al. (1973), Coutts et al. (1974), and Crothers & Cole (1978) for a review]. Tranfer RNA fragments have also permitted assignment of various NMR resonances in the intact tRNA and have provided information on the conformation of the whole tRNA molecule as well [see Kearns & Shulman (1974), Kim et al. (1977), and Robillard (1978) and references cited therein]. Recently, Boyle et al. (1980) studied the solution conformation of successively longer fragments of mature yeast $tRNA^{Phe}$ with a common 5′ end by NMR spectroscopy. They observed that only the stems found in intact yeast $tRNA^{Phe}$ are found in the fragments—no additional or competing helical regions are formed. Their results suggest that correct, sequential folding of the helical stems occurs before the entire molecule is synthesized.

In this paper, we use the temperature-jump method [summarized in Riesner et al. (1973) and Crothers & Cole (1978)] to examine the conformational equilibria and kinetics of the three yeast $tRNA^{Phe}$ fragments studied by Boyle et al. (1980). The fragments are (a) the 5′ $^1/_4$ fragment containing nucleotides 1–16, (b) the 5′ $^1/_2$ fragment containing nucleotides 1–36, and (c) the 5′ $^3/_5$ fragment containing nucleotides 1–45. Our results confirm the previous NMR findings and show that the order of melting of helices in the 5′ $^3/_5$ fragment is the anticodon helix followed by the D stem. This latter finding clarifies an ambiguity in earlier structural assignments of the melting transitions in yeast $tRNA^{Phe}$ (Crothers & Cole, 1978; Johnston & Redfield, 1981; Privalov & Filimonov, 1978; Hinz et al., 1977; Kan et al., 1977).

Experimental Procedures

Chemicals. Yeast phenylalanine-accepting tRNA was purchased from Boehringer Mannheim and used as a starting material for fragment preparation without further purification. All other chemicals were reagent grade.

tRNA Fragments. Yeast $tRNA^{Phe}$ fragments were prepared as described previously (Boyle et al., 1980). The 5′ $^1/_4$ (nucleotides 1–16) and 5′ $^1/_2$ (nucleotides 1–36) fragments were dialyzed vs. deionized water, lyophilized, and redissolved in 0.04 M sodium cacodylate (pH 6.8) and 1 mM ethylenediaminetetraacetic acid (EDTA). Samples of the 5′ $^3/_5$ fragment (nucleotides 1–45) were dialyzed against the same buffer.

Temperature-Jump Experiments. The temperature-jump instrument was basically similar to the double-beam design described by Crothers (1971). Modifications included a Schoeffel lamp housing with remote air cooling, a Schoeffel GM 250 monochromator, and continuous monitoring of both reference and sample beans with digital panel meters. The relaxation signals were displayed on a Tektronix oscilloscope using a 7A13 differential amplifier and a 7B50 time base. Single beam operation was used for signals less than 100 μs. The sample cell design was described by Cole (1972). The cell was constructed of Kel-F plastic with solid gold electrodes and had a volume of 1.4 mL with an optical path length of 0.7 cm. The temperature of the cell was measured with a T33A8 Victory Engineering thermistor probe inserted into the upper electrode. Temperature jumps of 1.5 °C were produced by the discharge of a 0.02-μF capacitor charged to 20 kV. The temperature-jump size was calibrated by the method of Havsteen (1969).

Because of the high-intensity light source (200-W Hg–Xe lamp), sample exposure was kept below 30 min for all RNA samples as previously described (Cole & Crothers, 1972). Frequent comparison of the behavior of exposed with fresh samples was also used to guard against artifacts arising from photomodification.

NMR Measurements. The NMR experiments have been described in detail in Boyle et al. (1980). Low-field data on the fragments were collected in a continuous wave mode on a Bruker HXS-360 NMR spectrometer. The temperature of the sample was controlled to ±1 °C. The NMR melting range of the helices present in each fragment sample corresponded

† From the Department of Biochemistry, Mississippi State University, Mississippi State, Mississippi 39762 (J.A.B.), the Department of Molecular Biophysics and Biochemistry, Yale University, New Haven, Connecticut 06510 (P.E.C.), and the Department of Chemistry, University of California, Berkeley, California 94720 (S.-H.K.). *Received August 19, 1982.* This work was supported by research grants from the National Institutes of Health to P.E.C. (GM 26109 and GM 21352) and to S.-H.K. (GM-31616), from the National Science Foundation to S.-H.K. (PCM 801-9468), and from the Mississippi Agricultural and Forestry Experiment Station to J.A.B. (MIS-6803). This is MAFES Contribution No. 5245.

‡ National Institutes of Health Career Development Awardee (GM 00471). Present address: Albert Einstein College of Medicine, Bronx, NY 10461.

0006-2960/83/0422-0741$01.50/0

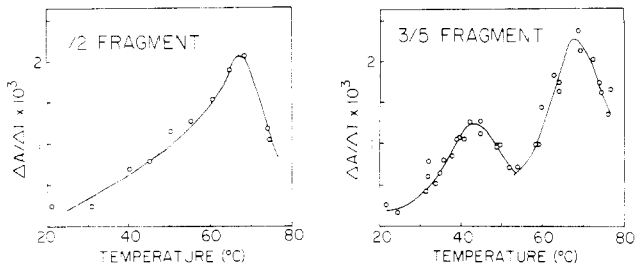

FIGURE 1: Differential melting curves of the 5′ $^3/_5$ and the 5′ $^1/_2$ fragments of yeast tRNA^{Phe}. The total amplitude (ΔA) for each effect was obtained from the zero-time intercept of the semilogarithmic plot of the absorbance change and was divided by the temperature-jump size (1.5 °C). The resultant $\Delta A/\Delta T$ was then plotted vs. the temperature corresponding to the midpoint of the temperature jump. Sample absorbances were 1 A_{266} unit/mL at 23 °C. All absorbance changes were monitored at 266 nm. The initial light intensity was 5000 mV for each jump.

Table I: Thermodynamic Properties of the Melting Transitions of Yeast tRNA^{Phe} Fragments and NMR Mapping Assignments

fragment transition	T_m (°C)[a]	ΔH^b (kcal/mol)	E^D_{act}[c] (kcal/mol)	structural assignment from NMR mapping
5′ $^1/_2$ in 0.04 M Na^+	67 ± 2	48 ± 10	39 ± 5	D stem
5′ $^3/_5$ in 0.04 M Na^+				
transition 1	43 ± 2	54 ± 10	54 ± 5	anticodon
transition 2	67 ± 2	45 ± 10	38 ± 5	D stem

[a] Defined as the temperature at the maximum of the differential melting curve (Figure 1). [b] Determined from the differential melting curves as described by Riesner et al. (1970). [c] Dissociation activation energies were determined from the mapping lines in Figures 2 and 3.

to the temperature range in which the initial resonance line widths doubled (see Results and Discussion). The NMR spectra in Figures 5 and 6 of Boyle et al. (1980) were used to obtain these data.

Results and Discussion

Thermodynamics and Relaxation Kinetics of Fragment Melting. For the 5′ $^1/_4$ fragment, a very fast relaxation effect (less than 5 μs) occurred at all temperatures. The time constant was too rapid to be measured by the temperature-jump (T-jump) method even when higher ionic strength solutions were used to reduce the heating time to less than 1 μs. The time scale of this absorbance change is consistent with single-strand unstacking and implies a lack of any appreciable secondary structure in the 5′ $^1/_4$ fragment (Crothers et al., 1974; Riesner et al., 1970).

Aside from single-strand unstacking, the melting of the 5′ $^1/_2$ fragment showed one resolvable relaxation effect whereas the 5′ $^3/_5$ fragment displayed two relaxation effects moderately well separated on the temperature scale. Figure 1 shows the temperature variation of the amplitude of the absorbance change associated with these fragments' relaxation effects. Since the amplitude of the relaxation effect corresponding to a helix–coil melting transition reaches a maximum at the T_m of that transition (assuming constant T-jump size), we have taken the T_m value for each transition as the temperature at the maximum of the corresponding differential melting curve in Figure 1. The values are listed in Table I.

Figures 2 and 3 show the temperature dependence of the time constants for each of the relaxation effects seen in Figure 1. The curves show the characteristic pattern for the melting

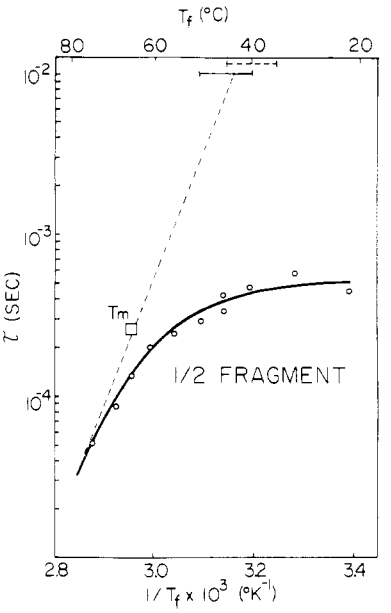

FIGURE 2: Variation of the 5′ $^1/_2$ yeast tRNA^{Phe} fragment relaxation time with reciprocal temperature in 0.04 M Na^+. Sample absorbance was 1 A_{266} unit/mL at 23 °C, and kinetics were monitored at 266 nm. T_f is the final temperature after the temperature jump. A line representing $1/k_D$ has been drawn through the high-temperature τ values and 2τ at $T = T_m$ and extrapolated back to the temperature at which $1/k_D = 10$ ms. T_m is represented by (□). A solid horizontal bar at the 10-ms level indicates the temperature where a 2-fold broadening is observed for the NMR resonances of this fragment's helix (the melting of resonances in this fragment occurred between 40 and 50 °C; see Experimental Procedures). A dashed horizontal bar represents the NMR melting range corrected maximally for the presence of a slightly higher Na^+ concentration in the NMR sample (see text). The dashed bar should also be at the 10-ms level but is offset in the figure for clarity.

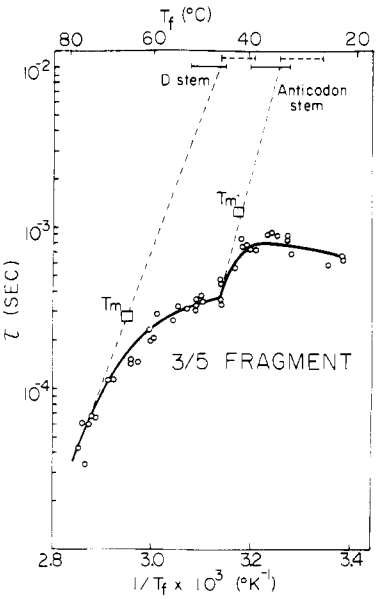

FIGURE 3: Variation of the 5′ $^3/_5$ yeast tRNA^{Phe} fragment relaxation times with reciprocal temperature in 0.04 M Na^+. Sample absorbance was 1 A_{266} unit/mL at 23 °C, and kinetics were monitored at 266 nm. T_f is the final temperature after the temperature jump. The lines and bars were drawn as described in the legend to Figure 2. T_m is represented by (□). The NMR melting for this fragment occurred in the range of 32–40 °C for the anticodon stem resonances and 45–52 °C for the D-stem resonances.

of RNA helices [see Crothers et al. (1974), Coutts et al. (1974), and Riesner & Römer (1973) and references cited therein]: the relaxation times are almost independent of

temperature for the lowest temperatures at which they are detected; τ decreases sharply as the T_m value of each transition is passed.

Since the 5′ $^1/_2$ fragment shows a single relaxation effect and the relaxation times for the 5′ $^3/_5$ fragment are moderately well separated on the time axis and temperature scale, each transition can be thought of as corresponding to a transition between helix and coil states. Within this approximation, we have calculated the enthalpy change for each effect from the differential melting curves by the procedure of Riesner et al. (1970). The values are tabulated in Table I. They are within the range of values previously reported from calorimetric studies of intact tRNA^{Phe} and optical melting of tRNA^{Phe} fragments (Freire & Biltonen, 1978; Privalov & Filimonov, 1978; Hinz et al., 1977; Riesner et al., 1973; Römer et al., 1969). Note also in Table I the correspondence in T_m values at 0.04 M [Na^+] between the 5′ $^1/_2$ fragment transition and transition 2 of the 5′ $^3/_5$ fragment. These results suggest that the helix which melts in transition 2 of the 5′ $^3/_5$ fragment is the helix which is present in the 5′ $^1/_2$ fragment.

NMR Mapping. The NMR studies of Boyle et al. (1980) indicated that the 5′ $^1/_2$ fragment contained the D stem and that the 5′ $^3/_5$ fragment contained both the D stem and the anticodon helix. The optical transitions detected here by relaxation methods indicate that the 5′ $^1/_2$ fragment contains one structured region while the 5′ $^3/_5$ fragment contains two, the second of which appears to correspond to that in the 5′ $^1/_2$ fragment by comparison of their T_m's. A confirmation of the identity of the helical structures which melt in these fragments and a clear determination of the order of helix melting in the 5′ $^3/_5$ fragment can be obtained by using the NMR mapping procedure developed by Crothers et al. (1974). This procedure combines NMR melting results with relaxation data.

When the NMR method is used to measure thermal unfolding of helices, the quantity observed is increased exchange of H-bonded ring NH protons with solvent water as the structure melts. A simple model for the process is

$$\text{helix} \underset{k_R}{\overset{k_D}{\rightleftharpoons}} \text{coil} \xrightarrow{k_{ex}} \text{exchange} \qquad (1)$$

As the temperature is raised, the ring NH hydrogen bonds become labile and the proton resonance broadens or disappears, so-called NMR melting (Crothers et al., 1973).[1] Under our buffer conditions, ring NH proton exchange with water occurs every time the helix is open (e.g., $k_{ex} \gg k_D$), and there is fast exchange between the helix and coil states on the NMR time scale.[2] In such a situation, the helix lifetime ($1/k_D$) determines the line broadening of the ring NH protons [see Crothers et al. (1974)]. The line broadening ($\delta\nu$) is related to $1/k_D$ by the relations

$$1/k_D = \pi\delta\nu \qquad (2)$$

where

$$\delta\nu = \Delta\nu - \Delta\nu_0 \qquad (3)$$

$\Delta\nu_0$ is the line width in the absence of broadening, and $\Delta\nu$ is the observed width (Crothers et al., 1974). Commonly, a doubling of line width is used as a measure of broadening, and for the NMR spectra of the tRNA^{Phe} fragments (Boyle et al., 1980), $\Delta\nu_0$ was 30 Hz. From this $\Delta\nu_0$ value and eq 2 and 3, the helix dissociation lifetime $1/k_D$ is approximately 10 ms at the temperaure where a resonance has broadened by a factor of 2. [Earlier work on oligonucleotides and tRNA took $\Delta\nu_0$ = 60 Hz and $1/k_D$ = 5 ms (Crothers et al., 1973, 1974; Hilbers et al., 1976; Robillard et al., 1977)]. Figures 2 and 3 show the NMR "melting" temperature, drawn as a solid bar at the 10-ms level, where we observed broadening from various sets of helical proton resonances in each of the fragments.

A structural assignment of the optical melting effects can now be made by correlating the helix lifetime of the fragment structures in the NMR data (whose identities are known from their NMR spectra) with the helix lifetime measured by relaxation kinetics. For the two-state transition between helix and coil shown in eq 2, the relaxation time (τ) is related to the rate constants by

$$1/\tau = k_D + k_R \qquad (4)$$

The τ values on the high-temperature side of T_m are dominated by the strongly temperature-dependent helix dissociation rate constant k_D while the τ values on the low-temperature extreme of a given transition reflect the temperature independence of the reassociation rate constant k_R (Cole & Crothers, 1972). Since $k_D = k_R$ at T_m and therefore $2\tau = 1/k_D = 1/k_R$, an asymptotic line drawn through 2τ at $T = T_m$ and the high-temperature τ values represents $1/k_D$ (see Figures 2 and 3). Therefore, this $1/k_D$ line upon extrapolation should intersect the 10-ms line in the NMR melting range for the helix that corresponds to the relaxation effect. As shown in Figures 2 and 3 and summarized in Table I, these NMR mapping lines indicate that the 5′ $^1/_2$ fragment's optical transition is the melting of the D stem, while for the 5′ $^3/_5$ fragment, the first transition is the anticodon melting and the second, higher temperature transition is the disruption of the D stem. There is no ambiguity in the mapping of the fragments' optical transitions since the following constraints on the mapping lines are met: (a) the line passes through 2τ at T_m and the high-temperature τ values; the slope of that line yields an activation energy for k_D (E_{act}^D) which is in reasonable agreement with ΔH of melting as seen in Table I (since k_R is nearly temperature independent, $\Delta H \approx E_{act}^D$); (b) each NMR melting range is associated with only one optical relaxation effect.

The estimated uncertainty in the NMR melting temperature, indicated by the breadth of the horizontal bars in Figures 2 and 3, deserves comment. The solid bar includes the uncertainty in the NMR melting temperature. The dashed bar shows this uncertainty and in addition has been shifted slightly as described below to take into account small differences in salt concentration between NMR and T-jump samples. The NMR sample was initially dialyzed against distilled water and then lyophilized and redissolved in buffer containing [Na^+] = 40 mM. However, because of the Donnan effect, the dialyzed tRNA fragments retain Na^+ ions at approximately 0.76 times the number of phosphate groups in the fragment (Felsenfeld & Miles, 1967) prior to addition of buffer. Thus, for the 5′ $^1/_2$ fragment, the sodium ion concentration of the NMR buffer was approximately 67 mM; for the 5′ $^3/_5$ frag-

[1] For all the fragments reported here, $1/k_D$ is much less than 5–10 ms at the optical T_m, k_{ex} is limited by k_D, and the resonances disappear with broadening at much lower temperatures than the optical T_m. In other reported situations, $1/k_D$ is much greater than 5–10 ms at the optical T_m, and k_{ex} is not determined by k_D; in those cases, the resonances do not broaden but rather disappear in proportion to the fraction of molecules that remain in the helix state (Crothers et al., 1973; Hilbers et al., 1976).

[2] When $\tau k_{ex} \gg 1$ where $1/\tau = k_R + k_D$, exchange with water occurs whenever the helix is open (Crothers et al., 1974). From the pK_a difference between uracil and cacodylate and at our buffer conditions of 40 mM sodium cacodylate, pH 6.8, we estimate the $k_{ex} \approx 5 \times 10^5$ s^{-1} (Cantor & Schimmel, 1980). Near the NMR melting temperatures of the fragments, $\tau = 2.6 \times 10^{-4}$ s for the 5′ $^1/_2$ fragment transition and the second transition of the 5′ $^3/_5$ fragment. For the first transition of the 5′ $^3/_5$ fragment, $\tau \simeq 1.3 \times 10^{-3}$ s. Thus, $\tau k_{ex} \gg 1$ for all of our transitions, and broadening of the ring NH protons is determined by $1/k_D$.

ment, the [Na^+] is approximately 74 mM. In the case of the T-jump samples, the concentration of fragment was substantially lower (by about 10^2) than in the NMR work, and the contribution of Donnan effect ions to the [Na^+] of the buffer is negligible. Values of $dT_m/(d \log [Na^+])$ for tRNA hairpin helices range from 8 to 23 °C (Cole et al., 1972). Recent estimates of $dT_m/(d \log [Na^+])$ for long RNA helices gave 8.4 °C for 100% GC and 13.5 °C for 48–57% GC, with short helices having a weaker dependence on ionic strength (Steger et al., 1980). Given that the [Na^+] of the T-jump samples is lower than that for the NMR samples and taking the worst possible case of $dT_m/(d \log [Na^+]) = 23$ °C, we determined that the relaxation curves of Figures 2 and 3 should be shifted to T_m values 5 °C higher for the 5′ $^1/_2$ fragment and 6 °C higher for the 5′ $^3/_5$ fragment for mapping to be done with all data at comparable salt conditions. Equivalently, the NMR melting bars should be shifted to lower temperature values by those amounts. We show the corrected NMR melting bars as dashed bars in Figures 2 and 3. The mapping lines intersect both the corrected and uncorrected NMR melting bars, leaving no inconsistency in our mapping conclusions.

These results confirm the conclusions of Boyle et al. (1980) concerning the sequential appearance of secondary structure in (yeast) $tRNA^{Phe}$. The common 5′-ended fragments used here mimic the synthesis of the nucleic acid. It is clear that the hairpin helices corresponding to those in the native $tRNA^{Phe}$ are formed when their component sequences are present in the molecule.

Stability of the Yeast $tRNA^{Phe}$ D Stem. Our result that the D stem melts after the anticodon helix provides an important clarification of conflicting results on the order of thermal unfolding steps for yeast $tRNA^{Phe}$. Previous T-jump studies with intact $tRNA^{Phe}$ and $tRNA^{Phe}$ half-molecules indicated that the D stem melted last (Coutts et al., 1975; Römer et al., 1969). On the basis of calorimetric studies of intact $tRNA^{Phe}$, Hinz et al. (1977) and Privalov & Filimonov (1978) have proposed that the D stem melts before the anticodon and TΨC stems. There is also some suggestion of an early D stem melting from the results of chemical modification experiments on yeast $tRNA^{Phe}$ (Rhodes, 1977). Johnston & Redfield (1981), using NMR proton exchange measurements, have very tentatively placed the D stem melting before the anticodon and TΨC stem melting although they state that they lack sufficiently good markers for the D stem to be certain about its position in the melting sequence. The 5′ $^3/_5$ fragment studied here was not used in previous thermal denaturation studies of yeast $tRNA^{Phe}$. Since it contains both the D-stem and anticodon helices, our mapping results on this fragment clearly show that the D stem melts after the anticodon stem, consistent with the findings of Maass and co-workers (Coutts et al., 1975; Römer et al., 1969).

The D-stem T_m values reported here for the 5′ $^1/_2$ and 5′ $^3/_5$ fragments as well as the D-stem T_m values previously reported for intact yeast $tRNA^{Phe}$ and its 5′ half-fragment (Coutts et al., 1975; Römer et al., 1969) are anomalously high compared with predictions based on properties of model oligonucleotides when allowance is made for solution conditions (Crothers et al., 1974; Crothers & Cole, 1978). In most other cases, the observed stability of tRNA hairpin helices has been in good accord with such predictions (Crothers & Cole, 1978). In addition, in $tRNA_f^{Met}$ (*Escherichia coli*) which has a D stem identical in sequence but reversed in polarity compared to the D stem of yeast $tRNA^{Phe}$, the D stem is apparently the first hairpin to melt (Crothers et al., 1974). From integration of the differential melting curves in Figure 1, the $tRNA^{Phe}$ D stem has a greater hypochromism than the anticodon stem, an unexpected result given the shorter D-helix length and the base-pair composition of both hairpins (Bloomfield et al., 1974; Fresco et al., 1963). This finding indicates that the D stem in our fragments is stabilized by more than just the 4 base pairs of the helix. This additional structure is completely coupled to the D stem melting kinetically, is not due to aggregation (data not shown), and does not appear to involve any ring NH protons in the NMR measurements (Boyle et al., 1980). The actual molecular structures (possibly involving adjacent loop sequences or dangling end sequences) which are responsible for the anomalously high stability of the yeast $tRNA^{Phe}$ D stem and for the differences in yeast $tRNA^{Phe}$ and $tRNA_f^{Met}$ (*Escherichia coli*) D-stem stabilities remain to be established.

References

Bloomfield, V. A., Crothers, D. M., & Tinoco, I. (1974) *Physical Chemistry of Nucleic Acids*, pp 295–301, Harper and Row, New York.

Boyle, J. A., Robillard, G. T., & Kim, S.-H. (1980) *J. Mol. Biol. 139*, 601–625.

Cantor, C. R., & Schimmel, P. R. (1980) in *Biophysical Chemistry*, pp 1166–1173, W. H. Freeman and Co., San Francisco, CA.

Cole, P. E. (1972) Ph.D. Thesis, Yale University, New Haven, CT.

Cole, P. E., & Crothers, D. M. (1972) *Biochemistry 11*, 4368–4374.

Cole, P. E., Yang, S. K., & Crothers, D. M. (1972) *Biochemistry 11*, 4358–4368.

Coutts, S. M., Gangloff, J., & Dirheimer, G. (1974) *Biochemistry 13*, 3938–3948.

Coutts, S. M., Riesner, D., Römer, R., Rabl, C. R., & Maass, G. (1975) *Biophys. Chem. 3*, 275–289.

Crothers, D. M. (1971) in *Procedures in Nucleic Acid Research* (Cantoni, G. L., & Davies, D. R., Eds.) Vol. 2, pp 369–388, Harper and Row, New York.

Crothers, D. M., & Cole, P. E. (1978) in *Transfer RNA* (Altman, S., Ed.) pp 196–247, MIT Press, Cambridge, MA.

Crothers, D. M., Hilbers, C. W., & Shulman, R. G. (1973) *Proc. Natl. Acad. Sci. U.S.A. 70*, 2899–2901.

Crothers, D. M., Cole, P. E., Hilbers, C. W., & Shulman, R. G. (1974) *J. Mol. Biol. 87*, 63–88.

Felsenfeld, G., & Miles, H. T. (1967) *Annu. Rev. Biochem. 36*, 407–448.

Freire, E., & Biltonen, R. (1978) *Biopolymers 17*, 1257–1272.

Fresco, J. R., Klotz, L. C., & Richards, E. G. (1963) *Cold Spring Harbor Symp. Quant. Biol. 28*, 83–90.

Havsteen, B. H. (1969) in *Physical Principles and Techniques of Protein Chemistry*, Part A, p 272, Academic Press, New York.

Hilbers, C. W., Robillard, G. T., Shulman, R. G., Blake, R. D., Webb, P. K., Fresco, J., & Riesner, D. (1976) *Biochemistry 15*, 1874–1882.

Hinz, H.-J., Filimonov, V. V., & Privalov, P. P. (1977) *Eur. J. Biochem. 72*, 79–86.

Johnston, P. D., & Redfield, A. G. (1981) *Biochemistry 20*, 3996–4006.

Kan, L. S., Ts'o, P. O. P., Sprinzl, M., von der Haar, F., & Cramer, F. (1977) *Biochemistry 16*, 3143–3154.

Kearns, D. R., & Shulman, R. G. (1974) *Acc. Chem. Res. 7*, 33–39.

Privalov, P. L., & Filimonov, V. V. (1978) *J. Mol. Biol. 122*, 447–464.

Rhodes, D. (1977) *Eur. J. Biochem. 81*, 91–102.

Riesner, D., & Römer, R. (1973) in *Physico-chemical Prop-*

erties of Nucleic Acids (Duchesne, J., Ed.) Vol. 2, pp 237-320, Academic Press, New York.
Riesner, D., Römer, R., & Maass, G. (1970) *Eur. J. Biochem. 15*, 85-91.
Riesner, D., Maass, G., Thiebe, R., Philippsen, P., & Zachau, H. G. (1973) *Eur. J. Biochem. 36*, 76-88.
Robillard, G. T. (1978) in *NMR in Biology* (Shulman, R., Ed.) pp 201-230, Academic Press, New York.
Robillard, G. T., Tarr, C., Vosman, F., & Reid, B. (1977) *Biochemistry 16*, 5261-5273.
Römer, R., Riesner, D., Maass, G., Wintermeyer, W., Thiebe, R., & Zachau, H. G. (1969) *FEBS Lett. 5*, 15-19.
Steger, G., Müller, H., & Riesner, D. (1980) *Biochim. Biophys. Acta 606*, 274-284.
Wintermeyer, W., Thiebe, R., Zachau, H. G., Riesner, D., Römer, R., & Maass, G. (1969) *FEBS Lett. 5*, 23-27.

Quantitation of Pyrimidine Dimer Contents of Nonradioactive Deoxyribonucleic Acid by Electrophoresis in Alkaline Agarose Gels†

Betsy M. Sutherland* and Alice G. Shih

ABSTRACT: We have developed a method of quantitating the pyrimidine dimer content of nonradioactive DNAs. DNA samples are treated with the UV-endonuclease from *Micrococcus luteus* and then separated according to molecular weight by electrophoresis on alkaline agarose gels. From their migration relative to known molecular weight standards, their median molecular weights and thus the number of dimers per DNA molecule in each sample can be calculated. Results of action spectra for dimer formation in T7 bacteriophage measured by this method agree well with action spectra for T7 killing. In addition, the method gives dimer yields in good agreement with those obtained by others using alkaline sucrose gradient sedimentation.

Cis-syn cyclobutylpyrimidine dimers are major lesions induced in DNA by ultraviolet light (UV; 220-320 nm). Classical methods of pyrimidine dimer measurement require radioactive labeling for location and quantitation after subsequent chromatographic or sedimentation analysis. It is important to be able to measure UV-induced pyrimidine dimer levels in DNAs of cells or tissues not amenable to radioactive labeling.

Achey et al. (1979) developed a method for detecting pyrimidine dimers in nonradioactive DNA of fish cells: extracted DNAs were treated with the *Micrococcus luteus* UV-endonuclease [which makes a single-strand nick adjacent to each dimer (Ahmed & Setlow, 1977)] and electrophoresed in alkaline agarose (McDonell et al., 1977). Dimer formation was deduced from the decrease in molecular weight in endonuclease-treated UV-irradiated samples. They also used radioactively labeled *Escherichia coli* DNA to analyze dimer contents by using three methods: (a) alkaline sucrose gradient sedimentation; (b) acid hydrolysis and chromatography; (c) gel electrophoresis. Although they found that the DNA profiles on gels reflected the dimer contents measured by other methods, they could not obtain absolute molecular weights from their gel samples. Sutherland et al. (1980) obtained estimates of dimer contents from gel electrophoresis of nonradioactive human skin DNA by comparison of the mid positions of the DNA profiles with the migration distances of molecular weight standards.

To examine this method further, we have chosen "ideal" conditions for experimental and theoretical analysis: a homogeneous population of small DNA molecules, well-defined dosimetry, and irradiation with monochromatic light. We also used DNA concentrations and agarose gel concentrations to allow optimal separation and display of intact and cleaved molecules. We show that pyrimidine dimer determination by our analysis method gives accurate measures of dimer yields (i.e., comparable to those obtained by others by alkaline sucrose gradient sedimentation). The technique also gives results of sufficient precision for action spectroscopy; action spectra obtained by this method on T7 bacteriophage and its DNA implicate a nucleic acid as chromophore and agree well with those for phage killing.

Materials and Methods

Bacteriophage. T7 bacteriophage were obtained from F. W. Studier, Brookhaven National Laboratory, and grown on *Escherichia coli* AB2500. Viable virus titer was determined by plating a dilution of phage and 0.2 mL of *E. coli* in 2 mL of soft agar (10 g of Bactotryptone, 5 g of NaCl, and 7 g of Bacto Agar per L) over a hard agar base (10 g of tryptone, 5 g of NaCl, and 10 g of Bacto Agar per L). Plates were incubated overnight at room temperature.

Irradiation. Purified phage were diluted to 3.2×10^{10}/mL in 50 mM tris(hydroxymethyl)aminomethane (Tris), pH 8, and 200 mM NaCl. Two-milliliter samples were exposed with constant stirring to monochromatic radiation from a Johns' monochromator (Johns & Rauth, 1965); incident light was monitored with a silicon photodiode. Incident intensities (in photons per second) for the various wavelengths (in nanometers) were the following: 248, 1.29×10^{14}; 265, 1.89×10^{14}; 280, 1.84×10^{14}; 289, 4.48×10^{14}; 297, 1.76×10^{15}; 313, 2.44×10^{16}. Irradiations and intensity measurements at 313 nm were of light filtered through a thin Mylar filter to exclude shorter wavelengths.

DNA Analysis. After each sample was irradiated, a small amount was removed for determining phage survival (see above). The remaining phage were concentrated by centrifugation for 1 h in a Brinkmann microcentrifuge. The phage

† From the Biology Department, Brookhaven National Laboratory, Upton, New York 11973. *Received June 30, 1982; revised manuscript received November 3, 1982.* This research was supported by Grants CA-26492 and CA-23096 from the National Cancer Institute of the National Institutes of Health, by the National Institutes of Health, and by the U.S. Department of Energy.

0006-2960/83/0422-0745$01.50/0